Journal of Applied Polymer Science

Network Transformations of Highly Dispersed MMT/SBR Nanocomposites During Processing

Yannan Quan,[1,2] Yiqing Wang,[1,2] Youping Wu,[1,2] Ming Lu,[1,2] Chao Zha,[1,2] Xiaohui Wu,[1,2] Liqun Zhang[1,2]

[1]College of Material Science and Engineering, Key Laboratory of Beijing City for Preparation and Processing of Novel Polymer Materials, Beijing University of Chemical Technology, Beijing 100029, China

[2]College of Material Science and Engineering, State Key Laboratory of Organic/Inorganic Composites, Beijing University of Chemical Technology, Beijing 100029, China

Correspondence to: L. Zhang (E-mail: zhanglq@mail.buct.edu.cn)

ABSTRACT: A highly dispersed montmorillonite (MMT)/styrene-butadiene rubber (SBR) nanocomposite is prepared by combining the latex compounding method and spray-drying process. The MMT layers exhibit a nearly exfoliated structure in the spray-dried powder. But when subjected to strains higher than 40%, the sprayed powdered nanocomposite goes through an irreversible transformation of the MMT network, showing a dramatic decrease in the storage modulus. XRD, SEM, and high resolution transmission electron microscopy results confirm the structure transformation of the MMT/SBR nanocomposite during processing. With intensive shearing during milling, the MMT layers are oriented, and further aggregations are observed in the vulcanizate. The processing procedures greatly alter the structures of the MMT/SBR nanocomposite. © 2013 Wiley Periodicals, Inc. J. Appl. Polym. Sci. 130: 113–119, 2013

KEYWORDS: clay; elastomers; composites

Received 13 October 2012; accepted 3 February 2013; published online 8 March 2013
DOI: 10.1002/app.39119

INTRODUCTION

Layered silicates naturally have a laminar structure with a thickness of approximately 1 nm. Many efforts have been spent in preparing the layered silicates/polymer nanocomposites. Once a good dispersion of the layered silicates is achieved, the layered silicates/polymer nanocomposites exhibit superior mechanical properties, barrier properties, thermal stability, and flame retardance.[1–3]

The biggest challenge comes from the dispersion of the layered silicate minerals. There are generally three types of thermodynamically achievable structures[4] for hybrid composites: conventional composite, in which the silicate layers appear as tactoids; intercalated composite, in which the silicate layers exhibit fixed gallery distance owing to the intercalation of the modifier or polymer; and exfoliated composite, in which the silicate platelets are randomly distributed in the polymer matrix and are amorphous to X-ray. Among all these structures, the exfoliated hybrid composites would provide the best performance for the optimized filler elements.[4,5]

Various methods, such as melt compounding,[6,7] solution compounding,[8,9] and *in situ* polymerization,[10–12] have been developed to prepare the layered silicates/polymer nanocomposites. All these methods are based on the same idea that with a miscible system built up for the polymer and the organically modified silicate layers, an intercalated or exfoliated composite can be obtained. Various modification methods have been applied to adjust the surface properties of the silicate layers.[13–17] But unfortunately, because of the diverse intrinsic properties of the polymers, it became rather complex and difficult to build up a suitable system for each layered silicate/polymer composite, and only limited success was achieved.

By combining the latex compounding method (LCM) and spray-drying process, we have developed a novel strategy for the preparation of highly dispersed layered silicates/polymer nanocomposites. Results showed that the montmorillonite (MMT) layers were well dispersed in the nanocomposite and a nearly exfoliated structure was obtained.[18] With further investigation, the structure transformations in the prepared highly dispersed nanocomposite during processing were observed.

In this work, we reported the network transformations of the MMT layers in the highly dispersed MMT/styrene-butadiene rubber (SBR) nanocomposite with the intention to draw more attention to this topic. Such filler network transformations may greatly alter the structure in the final product, leaving it dramatically different from the structure in the nanomaterial.

Applied Polymer SCIENCE

Table I. Recipe for Modified MMT/SBR Composite

Ingredients	Loading (phr[a])
SBR	100
HTAB/MMT	4/20
ZnO	5
Stearic Acid (SA)	2
Accelerator D[b]	0.5
Accelerator DM[c]	0.5
Accelerator TT[d]	0.2
Antioxidant 4010NA[e]	1
Sulfur	2

[a]Parts per hundred rubber parts in weight.
[b]Diphenyl guanideine.
[c]2,2′-dibenzothiazole disulfide.
[d]Tetramethylthiuram disulfide.
[e]*N*-isopropyl-*N*′-phenyl-p-phenylenediamine.

EXPERIMENTAL

Materials

Sodium MMT mineral (Siping Liufangzi Aska Bentonite, China), with a cationic exchange capacity of 78 mequiv./100 g, was used. The organic modifier for MMT used in this research was hexadecyl trimethyl ammonium bromide (HTAB, Beijing Yili Chemical, China), and it was used as received. SBR latex (SBR-1502, styrene content 23 wt %, Jilin petrochemical, China) was used as received. The curing additives (listed in Table I) for the rubber compound were reagent-grade commercial products and were used as received without further purification.

Preparation Procedures

Pristine MMT mineral was dispersed in deionized water under vigorous stirring; the sediment was removed after the slurry was settled for 24 h. A stable MMT aqueous colloid suspension with a solid content of 1.6 wt % was obtained by further centrifuging (4000 rounds per minute) the slurry. Surface modification to the MMT layers was carried out in the aqueous suspension by adding HTAB water solution under stirring. The organically modified MMT aqueous suspension was then compounded with the SBR latex by means of LCM. The composition ratio of HTAB, MMT, and SBR was kept at 4 g/20 g/100 g.

The mixture of MMT suspension and SBR latex was fed to an air-atomizing spray-drier (Laboratory Spray Drier, B-290, BUCHI, Switzerland). The mixture was dispersed into fine droplets by compressed air through a 2-mm diameter two-fluid nozzle. Hot air was used as the drying medium. The inlet and outlet temperatures were 220 and 100°C, respectively, and the feeding rate was 200 mL/h. The spray-dried powder was collected, and the HTAB-modified MMT/SBR powdered compound (HTAB(4)/MMT(20)/SBR) was obtained.

Milled bulk compound was obtained by kneading the obtained powdered compound into a mass on a 6-in. two-roll miller. The milled bulk compound was further mixed with the curing additives (Table I) on the miller. After curing at 150°C for a period of 5 min (T_{90}, the optimum curing time) under the pressure of 15 MPa, the vulcanizate was obtained.

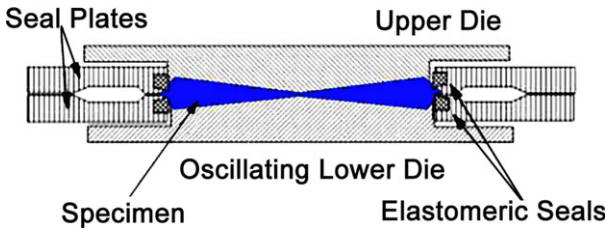

Figure 1. Die configuration of RPA 2000.[19] [Color figure can be viewed in the online issue, which is available at wileyonlinelibrary.com.]

A hot-pressed sample was prepared to investigate the effect of curing conditions on the aggregation of MMT layers. The sample was obtained from the milled bulk compound by further pressing under the curing conditions of 150°C, 15 MPa, and 5 min, with no curing agents added. The differences between the hot-pressed compound and the vulcanizate were that the vulcanizate sample underwent more intensive shearing during the mixing process and the vulcanization reactions took place only in the vulcanizate sample.

Characterization

Dynamical mechanical rheology measurements were performed with an RPA 2000 rheometer (Alpha Technologies, Akron, Ohio) at the temperature of 60°C and the frequency of 1 Hz. Approximately 4–5 g of powdered or bulk compound was loaded into the test cavity with two biconical dies (shown in Figure 1). When the upper die was closed by the compressed air (0.6 MPa), the preprogrammed rheological measurements were performed on the test specimen. Strain was applied by varying the oscillation angle. The torque was transmitted via the sample from the oscillating lower die to the highly sensitive torque transducer positioned in the upper die, and selected sample properties (torque and modulus) were measured at the preprogrammed frequency and temperature. There was an interval of 10 s between consecutive tests for sample conditioning.

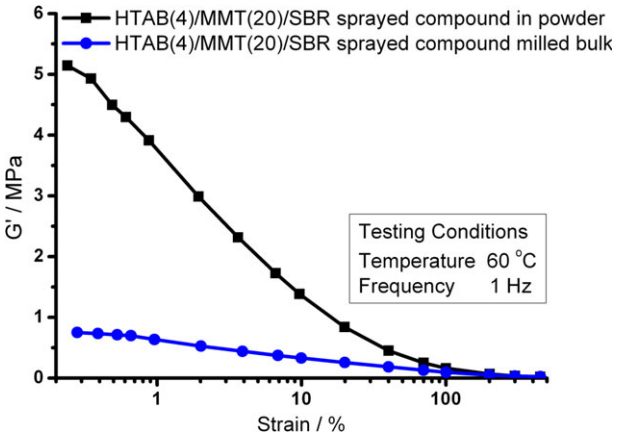

Figure 2. Strain amplitude dependence of storage modulus (G') of the HTAB(4)/MMT(20)/SBR sprayed powdered compound and milled bulk compound. [Color figure can be viewed in the online issue, which is available at wileyonlinelibrary.com.]

The morphologies of the freeze- and tensile-fractured surfaces of the spray-dried MMT/SBR composites were obtained on a Hitachi S-4700 scanning electron microscope (Hitachi, Japan) operated at 20 kV acceleration voltage. The samples for high resolution transmission electron microscopy (HR-TEM) were prepared by microtomy and then investigated with a JEM-3010 high resolution transmission electron microscope (JEOL, Japan) operated at 300 kV accelerating voltage. X-ray diffraction measurements were conducted on a D/Max2500 VB2+/PC X-ray diffractometer (Rigaku, Japan) with Cu/Kα1 radiation (λ = 0.154056 nm), and the diffraction patterns were recorded at 40 kV and 200 mA.

RESULTS AND DISCUSSION

MMT Network Detected by Dynamic Strain Sweeps

The Payne effect[20–22] is widely used to characterize the filler network in filled rubber compounds. The Payne effect describes the dependence of the storage modulus (G') of the filled rubber compound on the applied strain amplitude: the storage modulus decreases rapidly with increasing dynamic strain amplitude. Many studies[22] showed that the Payne effect is attributed to the formation of filler network by both filler–filler interactions and filler–rubber interactions and the subsequent deconstruction of the filler network by increasing strain.

Our experiments showed that the spray-dried HTAB-modified MMT/SBR nanocomposite exhibited an extraordinarily high modulus at small strain amplitudes, an indication that the MMT layers were highly dispersed in the SBR matrix to form a strong MMT network. However, after milling, a significant decrease in the storage modulus of the filled compound was observed, as shown in Figure 2, indicating a dramatic change in the filler network of the HTAB-modified MMT/SBR compound. Yang et al. observed a similar phenomenon in expanded graphite/rubber nanocomposite.[23] They also found that the electrical conductivity of the expanded graphite/rubber compound prepared by the LCM decreased significantly right after the compound was mechanically mixed. Such phenomena led us to further investigate the role the processing procedures played in determining the MMT network in the highly dispersed MMT/SBR nanocomposite.

Figure 3 shows the strain amplitude and time dependence of storage modulus (G') of the HTAB-modified MMT/SBR powdered compound under repeated strain sweeps. Results showed that the MMT network was greatly damaged after just one strain sweep at strain amplitudes up to 400%, and the network varied little during further repeated measurements. At 60°C for 1 h, the MMT network recovered to some extent, but it was far weaker than the original network in the powdered compound.

To explore in further detail the changes in the MMT network during the first strain sweep, we divided the strain sweep with strain amplitudes up to 400% into six cyclic strain sweep procedures with step changes in strain amplitude from 0.28–2% to 0.28–400%. The results are shown in Figure 4. The Payne effect is observed at every strain step. At strain amplitudes below 10%, the spray-dried HTAB-modified MMT(20)/SBR powdered compound shows an elastic behavior: the dynamic storage modulus fully recovers to its original value after the small-amplitude strain sweeps [Figure 4(a–c)]. However, when the strain amplitude increases to 40%, an irreversible damage to the MMT network is observed: the storage modulus cannot recover to the

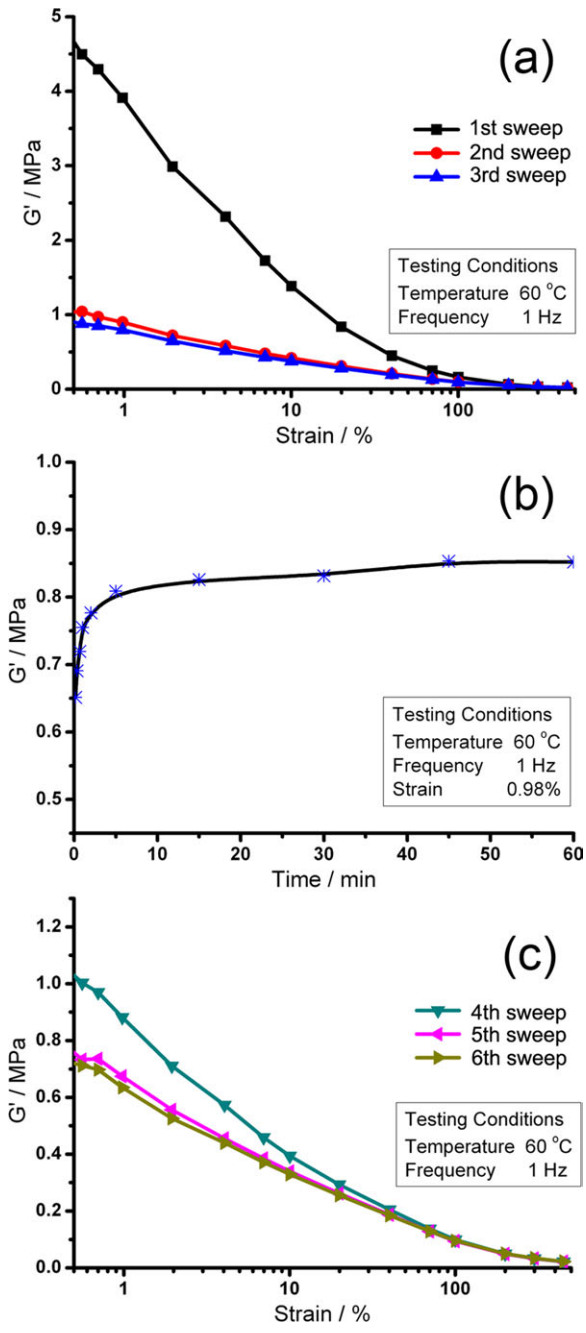

Figure 3. Strain amplitude and time dependence of storage modulus (G') of the HTAB(4)/MMT(20)/SBR sprayed powdered compound under repeated strain sweeps [(a) displays the initial strain sweep measurements for the spray-dried powdered compound, (b) displays a one-hour recovery process right after the initial strain sweeps, and (c) shows the three times strain sweep measurements following the recovery process]. [Color figure can be viewed in the online issue, which is available at wileyonlinelibrary.com.]

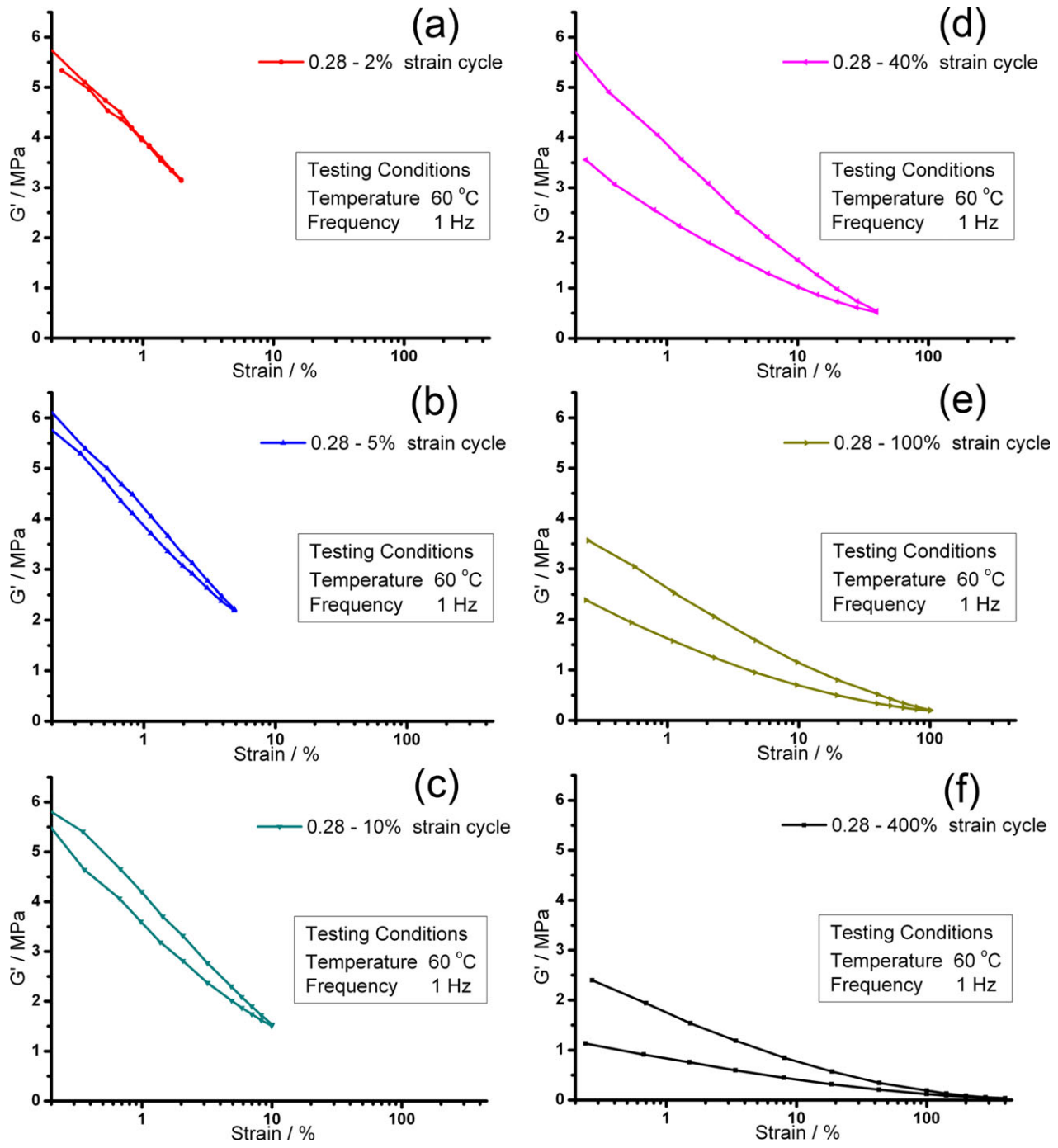

Figure 4. Strain amplitude dependence of storage modulus (G') of the HTAB(4)/MMT(20)/SBR sprayed powdered compound under cyclic strain sweeps with increasing strain amplitudes. [Color figure can be viewed in the online issue, which is available at wileyonlinelibrary.com.]

original value after the large-amplitude strain sweep. Such an irreversible damage goes further with the strain amplitude increasing up to 100 and 400%, as shown in Figure 4(d–f).

Simultaneously, a stress-softening effect, also known as the Mullins effect, is observed in the cyclic strain sweeps with stepped strain amplitudes, as revealed in Figure 5. During the test, three rounds of cyclic strain sweeps were conducted at each step change in strain amplitude. The Mullins effect agrees well with the Payne effect observed in the stepped cyclic strain sweeps. At strain amplitudes below 10%, the compound exhibits an elastic behavior, but at strain amplitudes above 40%, the compound shows a dramatic stress-softening effect (the stress decreases dramatically between the first cycle and subsequent cycles).

MMT Dispersion Transformation During Processing

By comparing the XRD patterns of the highly dispersed MMT/SBR nanocomposites at various processing stages, as displayed in Figure 6, we can also see the structure transformations. The patterns shown in Figure 6 are normalized by the diffraction

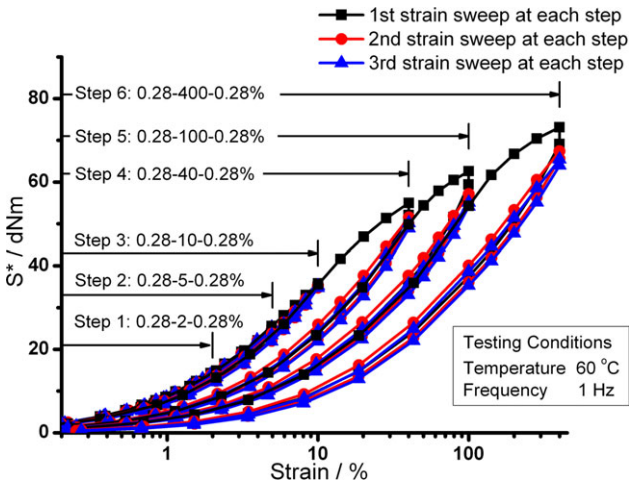

Figure 5. Strain amplitude dependence of complex torque (S^*) of the HTAB(4)/MMT(20)/SBR sprayed powdered compound under stepped cyclic strain sweeps. [Color figure can be viewed in the online issue, which is available at wileyonlinelibrary.com.]

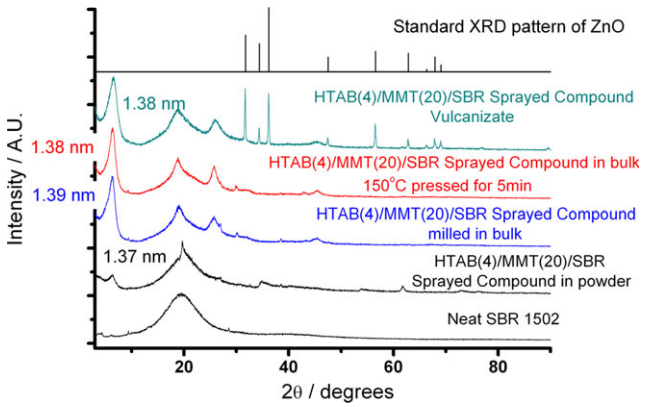

Figure 6. XRD patterns of HTAB(4)/MMT(20)/SBR nanocomposites at different processing stages. [Color figure can be viewed in the online issue, which is available at wileyonlinelibrary.com.]

peak of the SBR matrix at about 20°. The sprayed powdered MMT/SBR compound is nearly amorphous to X-rays, demonstrating the highly dispersed structure in the powdered compound. But after the processing procedures, the MMT/SBR compounds and vulcanizate show distinct diffraction peaks at about 6.5°, corresponding to the stacked MMT structures.

Further electron microscope observations reveal details in the MMT dispersion transformations during processing. As can be

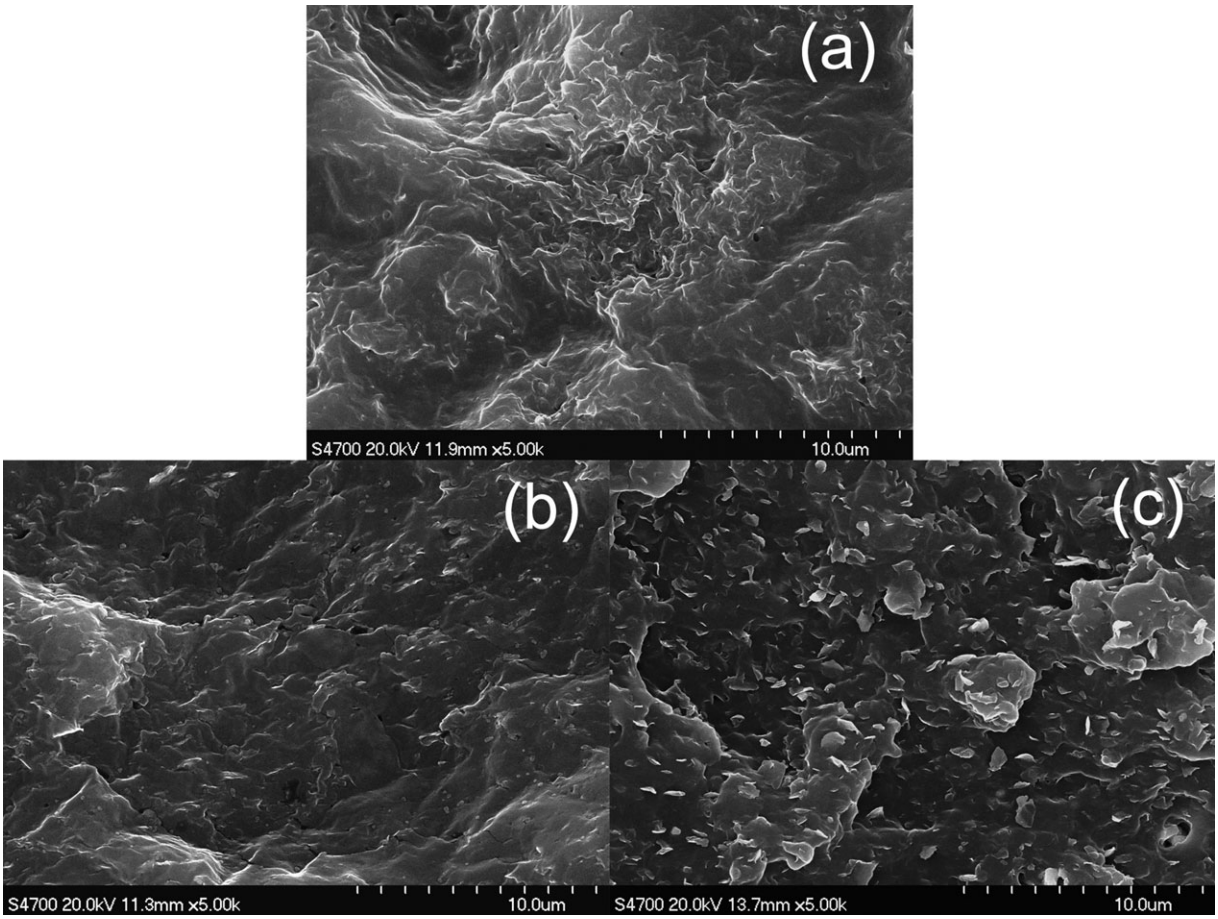

Figure 7. SEM images of fractured surfaces of the HTAB(4)/MMT(20)/SBR composites at different processing stages [(a) is the freeze-fractured surface of the sprayed powdered compound, (b) is the freeze-fractured surface of the milled bulk compound, and (c) is the tensile-fractured surface of the vulcanizate].

Applied Polymer SCIENCE

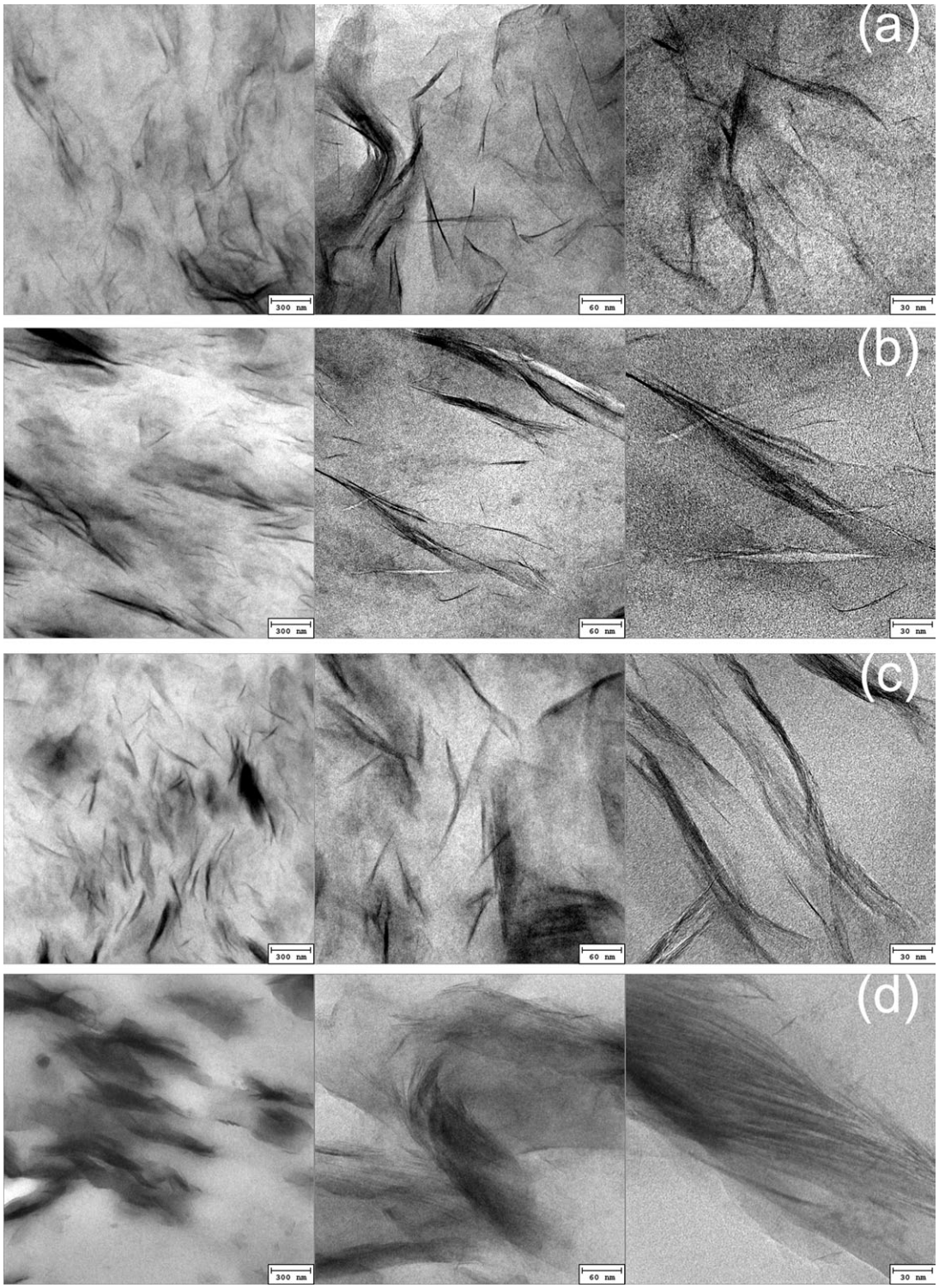

Figure 8. HR-TEM images of HTAB(4)/MMT(20)/SBR composites at different processing stages [(a), (b), (c), and (d) are the image sets for the spray-dried powdered compound, milled bulk compound, milled and hot pressed compound, and vulcanizate, respectively].

seen in Figure 7, the MMT layers in the sprayed powdered compound exhibit a roughly disordered structure; however, during processing, the MMT layers show orientations. The high-resolution TEM images shown in Figure 8 confirm this transformation. After milling and hot pressing, the MMT layers are oriented; with constant intensive shearing during mixing and high temperature and pressure during curing, the MMT layers exhibit dramatic aggregation in the MMT/SBR vulcanizate, showing a remarkably changed structure far different from that in the powdered compound.

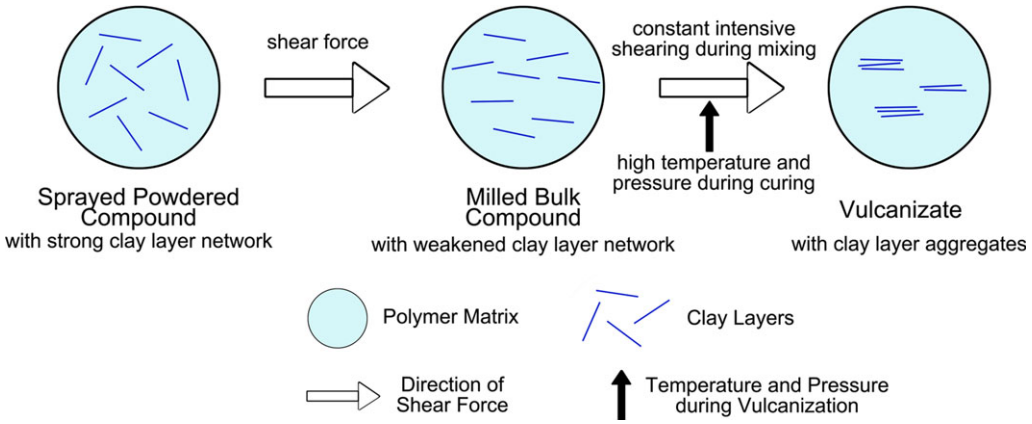

Figure 9. Schematic illustration of network transformations during processing. [Color figure can be viewed in the online issue, which is available at wileyonlinelibrary.com.]

Figure 9 schematically illustrates the MMT network transformations during processing. We believe it is the shear-induced orientations of the MMT layers that greatly change the network structures of the spray-dried MMT/SBR nanocomposite. The disordered MMT layers in the spray-dried powdered compound lead to extraordinarily strong network. However, after intensive shearing, the MMT network is damaged, and the oriented MMT layers form a weak network. The orientation of the MMT layers is also the first step to further aggregations. By the constant intensive shearing during mixing and high temperature and pressure during curing, the oriented MMT layers are more likely to aggregate and form face-to-face restacked structures.

CONCLUSIONS

MMT layers exhibited a nearly exfoliated structure in the spray-dried powder of MMT/SBR compound prepared by a combined method of latex compounding and spray-drying. However, the processing procedures greatly altered the structures of the MMT/SBR nanocomposite. Results from the RPA strain sweeps revealed that at strain amplitudes larger than 40%, the spray-dried MMT/SBR powdered compound went through an irreversible transformation of the MMT network, and the storage modulus of the compound dramatically decreased. XRD, SEM, and HR-TEM results confirmed the structure transformations of the MMT/SBR nanocomposite during processing. With intensive shearing during milling, the MMT layers were oriented, and aggregates of face-to-face restacked MMT layers were formed in the vulcanizate.

ACKNOWLEDGMENTS

The authors appreciate the financial supports from the National Science Fund for Distinguished Young Scholars (50725310), China and the National High Technology Research and Development Program 863 (2009AA03Z338), China.

REFERENCES

1. Pavlidou, S.; Papaspyrides, C. D. *Prog. Polym. Sci.* **2008**, *33*, 1119.
2. Sinha Ray, S.; Okamoto, M. *Prog. Polym. Sci.* **2003**, *28*, 1539.
3. Zanetti, M.; Lomakin, S.; Camino, G. *Macromol. Mater. Eng.* **2000**, *279*, 1.
4. LeBaron, P. C.; Wang, Z.; Pinnavaia, T. J. *Appl. Clay Sci.* **1999**, *15*, 11.
5. Giannelis, E. P. *Adv. Mater.* **1996**, *8*, 29.
6. Zhang, Y.-Q.; Lee, J.-H.; Rhee, J. M.; Rhee, K. Y. *Compos. Sci. Technol.* **2004**, *64*, 1383.
7. Arroyo, M.; López-Manchado, M. A.; Valentín, J. L.; Carretero, J. *Compos. Sci. Technol.* **2007**, *67*, 1330.
8. Kim, H. B.; Choi, J. S.; Lee, C. H.; Lim, S. T.; Jhon, M. S.; Choi, H. J. *Eur. Polym. J.* **2005**, *41*, 679.
9. Shen, Z.; Simon, G. P.; Cheng, Y.-B. *Polymer* **2002**, *43*, 4251.
10. Tsai, T.-Y.; Lin, M.-J.; Chang, C.-W.; Li, C.-C. *J. Phys. Chem. Solids* **2010**, *71*, 590.
11. Roy, N.; Bhowmick, A. K. *Polymer* **2010**, *51*, 5172.
12. Yilmaz, O.; Cheaburu, C. N.; Durraccio, D.; Gulumser, G.; Vasile, C. *Appl. Clay Sci.* **2010**, *49*, 288.
13. Kooli, F.; Liu, Y.; Alshahateet, S. F.; Messali, M.; Bergaya, F. *Appl. Clay Sci.* **2009**, *43*, 357.
14. Sarier, N.; Onder, E.; Ersoy, S. *Colloids Surf. A* **2010**, *371*, 40.
15. Yoon, K.-B.; Sung, H.-D.; Hwang, Y.-Y.; Noh, S. K.; Lee, D.-H. *Appl. Clay Sci.* **2007**, *38*, 1.
16. Bhiwankar, N. N.; Weiss, R. A. *Polymer* **2005**, *46*, 7246.
17. Livi, S.; Duchet-Rumeau, J.; Gérard, J.-F. *J. Colloid Interface Sci.* **2011**, *353*, 225.
18. Lu, M.; Wang, Y.; Wu, Y.; Quan, Y.; Wu, X.; Zhang, L.; Guo, B. *Macromol. Mater. Eng.* **2012**, *297*, 20.
19. ALPHATECHNOLOGIES, Die configuration of RPA 2000. Available at: http://www.alpha-technologies.com/stuff/contentmgr/files/1/5b1962d0005181da84edb18f203d3196/files/rpa2000_dieconfig.jpg (accessed January 9, 2013).
20. Payne, A. R. *J. Appl. Polym. Sci.* **1962**, *6*, 57.
21. Payne, A. R. *J. Appl. Polym. Sci.* **1962**, *6*, 368.
22. Allegra, G.; Raos, G.; Vacatello, M. *Prog. Polym. Sci.* **2008**, *33*, 683.
23. Yang, J.; Zhang, L.-Q.; Shi, J.-H.; Quan, Y.-N.; Wang, L.-L.; Tian, M. *J. Appl. Polym. Sci.* **2010**, *116*, 2706.